Improved search for elementary particles with fractional electric charge

Nancy M. Mar, Eric R. Lee, George R. Fleming,* Brendan C. K. Casey,† Martin L. Perl, and Edward L. Garwin
Stanford Linear Accelerator Center, Stanford, California 94309

Charles D. Hendricks
W. J. Schafer Associates, Livermore, California 94550

Klaus S. Lackner
Theoretical Division, Los Alamos National Laboratory, Los Alamos, New Mexico 87545

Gordon L. Shaw
Department of Physics, University of California, Irvine, California 92717
(Received 27 December 1995)

We have devised and demonstrated the successful operation of a low-cost, high-mass throughput technique capable of performing bulk matter searches for fractionally charged particles based on an improved Millikan liquid drop method. The method uses a stroboscopic lamp and a charge coupled device video camera to image the trajectories of silicone oil drops falling through air in the presence of a vertical, alternating electric field. The images of the trajectories are computer processed in real time, the electric charge on a drop being measured with an rms error of 0.025 of an electron charge. This error is dominated by Brownian motion. In the first use of this method, we have looked at 5 974 941 drops and found no evidence for fractional charges in 1.07 mg of oil. With 95% confidence, the concentration of isolated quarks with $\pm 1/3e$ or $\pm 2/3e$ in silicone oil is less than one per 2.14×10^{20} nucleons. [S0556-2821(96)00411-0]

PACS number(s): 14.65.−q, 06.20.Jr, 07.50.Yd

I. INTRODUCTION

We have conducted a search for elementary particles with fractional electric charge in silicone oil using an improved Millikan liquid drop method in which we automatically measure the charge on individual drops of about 7 μm in diameter. We have searched through 1.07 mg of oil and found no drops that contained a fractionally charged particle with $\pm\frac{1}{3}$ or $\pm\frac{2}{3}$ of an electron charge. Therefore, with 95% confidence the concentration of isolated quarks with these charges in silicone oil is less than one per 2.14×10^{20} nucleons.

There has been much speculation but no confirmed evidence for the existence of isolated elementary particles with fractional electric charge. The most commonly proposed candidate for such a particle is an isolated quark that would have charge $\pm\frac{1}{3}e$ or $\pm\frac{2}{3}e$, where e is the magnitude of the electric charge of the electron. In this experiment, drops are produced with a nominal charge of $0e$, $\pm1e$, $\pm2e$,.... In the early part of the experiment, drops were produced with charges as large as $\pm10e$, but in the remainder of the experiment, the drops were generally either neutral or had charges of $\pm1e$, $\pm2e$, or $\pm3e$. The sensitivity of the experiment for an anomalous charge decreases when Q, the net electric charge on the drop, is close to Ne, N being an integer. Therefore, our conclusions are limited to the charge regions

$$0.2e \text{ to } 0.8e,\ 1.2e \text{ to } 1.8e,\ 2.2e \text{ to } 2.8e\ldots$$
$$-0.2e \text{ to } -0.8e,\ -1.2e \text{ to } -1.8e,$$
$$-2.2e \text{ to } -2.8e,\ldots . \quad (1)$$

Our method is built upon the technique developed in fractional charge searches at San Francisco State University [1–4] and goes back to the original work of Millikan [5–7]. As shown schematically in Fig. 1, the mechanical part of the apparatus consists of two flat, circular, stainless-steel plates separated by a distance small compared with the plate diameter, the ratio being on the order of 1:16. A device called a dropper produces on demand a spherical drop of silicone oil whose diameter is between 7 and 8 μm. Early in the experiment, we produced drops that were 7.6 μm in diameter. But 94% of the drops studied had a diameter of 7.1 μm. The data presented in the paper is for both sizes, but for simplicity, the remainder of the discussion refers to the 7.1 μm drops.

The drops fall vertically through a small hole in the upper plate, through the space between the plates, and then leave

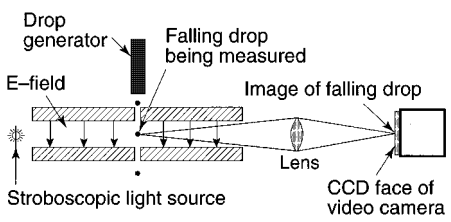

FIG. 1. Schematic of the fractional charge search apparatus. Drawing is not to scale.

*Present address: Department of Physics, Columbia University, New York, NY 10027.

†Present address: W. J. Schafer Associates, Livermore, CA 94550.

the apparatus through a small hole in the lower plate. The entire apparatus is in dry air at atmospheric pressure and room temperature. The frictional resistance of the air brings a 7.1-μm drop to terminal velocity within a few thousandths of a millimeter. The terminal velocity for a neutral drop of this size is 1.35 mm/s. The frequency of drop production was set at 0.6 Hz. A 7.1-μm-diam drop of silicone oil has a mass of 1.71×10^{-4} μg and contains 1.03×10^{14} nucleons.

Between the plates there is a uniform, vertical electric field. The field strength changes in time with a square wave oscillation amplitude of 1.4×10^{6} V/m. If the drop has a nonzero charge, the terminal velocity differs according to whether the electric field reinforces or opposes the gravitational force. By the means described next, we measure the terminal velocity in both situations and use the theory described in Sec. II to calculate the charge on the drop and the mass of the drop.

Continuing to refer to Fig. 1, a stroboscopic lamp illuminates the drop twice for each electric-field orientation and a lens images the shadow of the drop onto a charge coupled device (CCD) video camera. Thus, the position of the shadow of the drop on the CCD surface measures the position of the drop in real space when the stroboscopic lamp flashes. A desktop computer uses the output of the CCD camera to calculate the drop's terminal velocities, diameter, and charge. The computer also controls the experiment and stores the measurements.

The plan of the paper is as follows. The theory of the experiment is outlined in Sec. II. The construction of the apparatus is described in Sec. III. Collection, selection, and presentation of data and errors are discussed in Secs. IV and V. Our results are summarized and compared with other measurements in Sec. VI. Proposed improvements and extensions of the experimental technique as laid out in [8] are discussed in Sec. VII.

II. THEORY OF THE EXPERIMENT

Consider a drop falling under the influence of gravity and a vertical electric field that switches between two discrete states, up and down. By Stokes' law we have the two equations

$$mg+QE_{\text{down}}=6\pi\eta r v_{E_{\text{down}}}, \tag{2}$$

$$mg-QE_{\text{up}}=6\pi\eta r v_{E_{\text{up}}}, \tag{3}$$

where g is the acceleration due to gravity, Q is the net electric charge on the drop, $E_{\text{up,down}}$ is the magnitude of the applied electric field depending on whether the field points up or down, respectively, η is the dynamic viscosity of air, $v_{E_{\text{up}}}$ and $v_{E_{\text{down}}}$ are the terminal velocities of the drop corresponding to $E_{\text{up,down}}$, r is the radius of the drop, and m is the effective mass of the drop. The effective mass is given by $m=\frac{4}{3}\pi r^3(\rho_{\text{oil}}-\rho_{\text{air}})$, where ρ_{oil} is equal to 913 kg/m^3. Taking the sum of and the difference between Eqs. (2) and (3) yields the two equations

$$2mg+Q(E_{\text{down}}-E_{\text{up}})=6\pi\eta r(v_{E_{\text{down}}}+v_{E_{\text{up}}}), \tag{4}$$

$$Q=6\pi\eta r\left(\frac{v_{E_{\text{down}}}-v_{E_{\text{up}}}}{E_{\text{down}}+E_{\text{up}}}\right). \tag{5}$$

Substituting Eq. (5) into (4) gives an equation for the radius of the drop:

$$r=3\sqrt{\frac{\eta}{2g(\rho_{\text{oil}}-\rho_{\text{air}})}}\left(\frac{v_{E_{\text{up}}}V_{\text{down}}+v_{E_{\text{down}}}V_{\text{up}}}{V_{\text{down}}+V_{\text{up}}}\right)^{1/2}. \tag{6}$$

Here we have substituted $E_{\text{down}}=V_{\text{down}}/d$ and $E_{\text{up}}=V_{\text{up}}/d$, where $V_{\text{up,down}}$ is the applied voltage (±13 kV) and d denotes the separation between the electric field plates (9.4 mm). Substituting Eq. (6) into Eq. (5) yields the charge equation.

$$Q=9\pi d\sqrt{\frac{2\eta^3}{g(\rho_{\text{oil}}-\rho_{\text{air}})}}\left(\frac{v_{E_{\text{down}}}-v_{E_{\text{up}}}}{V_{\text{down}}+V_{\text{up}}}\right)\times\sqrt{\frac{v_{E_{\text{up}}}V_{\text{down}}+v_{E_{\text{down}}}V_{\text{up}}}{V_{\text{down}}+V_{\text{up}}}}. \tag{7}$$

To improve the precision and accuracy of our measurements, we explicitly include the dependence of η and ρ_{air} on ambient temperature and pressure. We define the function

$$F(T,P)=\sqrt{\frac{2}{g(\rho_{\text{oil}}-\rho_{\text{air}})}}\,\eta^{3/2}=\sqrt{\frac{2}{g(\rho_{\text{oil}}-cP/T)}}\left(\frac{aT^{3/2}}{b+T}\right)^{3/2}, \tag{8}$$

where $\rho_{\text{air}}=c(P/T)$ and $\eta=aT^{3/2}/(b+T)$ and parameters are given as $a=1.485\times10^{-6}$ kg m^{-1} s^{-1} K$^{-1/2}$, $b=110.4$ K, and $c=3.489\times10^{-3}$ kg K m^{-3} Pa^{-1}. The parameters P and T denote the ambient air pressure (Pa) and the ambient temperature (K), respectively. Equation (7) becomes

$$Q=9\pi dF(T,P)\left(\frac{v_{E_{\text{down}}}-v_{E_{\text{up}}}}{V_{\text{down}}+V_{\text{up}}}\right)\sqrt{\frac{v_{E_{\text{up}}}V_{\text{down}}+v_{E_{\text{down}}}V_{\text{up}}}{V_{\text{down}}+V_{\text{up}}}}. \tag{9}$$

III. APPARATUS

A. Drop generator

The part of the apparatus that has required the most development is the generator for producing small and uniform size oil drops. The design of the oil drop generator, called the dropper for the sake of brevity, is based on a combination of ideas for fluid drop ejectors originally developed at San Francisco State University [1–4] and Lawrence Livermore Laboratories. Nevertheless, we have had to make many improvements.

As shown in Fig. 2, the dropper consists of a brass tube with an inside diameter of 4.8 mm, wall thickness of 1.6 mm, and length of 6.4 cm. An annular piezoelectric transducer disk made from lead zirconate titanate with an inside diameter of 6.4 mm, outside diameter of 25.4 mm, and thickness of 2.5 mm is attached around the lower portion of the tube with epoxy. A 9.5-mm-diam stainless-steel orifice plate of 0.4 mm thickness with an 8-μm-diam concentric hole is affixed to the bottom of the dropper also with epoxy. The

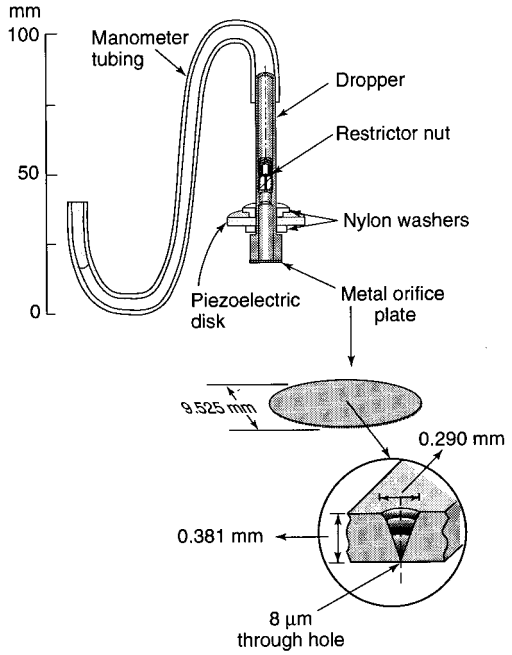

FIG. 2. Drawing of the dropper and of the orifice plate affixed to the bottom of the dropper. A cross section of the orifice plate is pictured at the lower right. It shows the conical features of the 8-μm hole that determines approximately the size of the drops. Dimensions for the orifice plate were obtained by studying the plate under an electron microscope. The slope of the conical sides of the orifice changes from approximately 32° from the vertical near the top to 20° from the vertical and finally to 18° from vertical.

8-μm-diam hole fixes approximately the diameter of the drop. The exact diameter depends on the voltage with which we pulse the transducer.

The dropper is filled with the silicone oil and placed under a low-grade vacuum for about $1\frac{1}{2}$ h. This is done so that air bubbles acquired during the filling process are removed. A plastic tube with an inner diameter of 4.8 mm and approximately 30 cm long is placed over the opening of the dropper and is likewise filled with oil. The end of the tube is varied in height relative to the bottom of the dropper to control the amount of relative pressure at the fluid meniscus of the ejection orifice (Fig. 2). The dropper holds approximately 6 g of oil that was changed about every 2×10^6 drops.

Drop ejection is initiated when the piezoelectric transducer contracts radially upon receiving an electrical pulse from the high-voltage pulse amplifier. This contraction squeezes the dropper and forces drop ejection. In our case, the transducer is pulsed at a driving voltage ranging from 130 to 160 V with a pulse width ranging from 0.85 to 1.2 μs. A restrictor nut sits inside the dropper so that there is a node for the pressure wave arising from the transducer pulse. The transducer then relaxes to its rest state until the next electrical pulse. The negative pressure wave caused by the relaxation of the piezoelectric material to its equilibrium state retracts the fluid into the dropper. The fluid column retraction takes place in the long conical column of the orifice hole, preventing air from being drawn into the main fluid chamber (Fig. 2). Capillary action then restores the meniscus, so that upon the next electrical pulse, drop ejection is once again initiated. A slightly negative manometer pressure

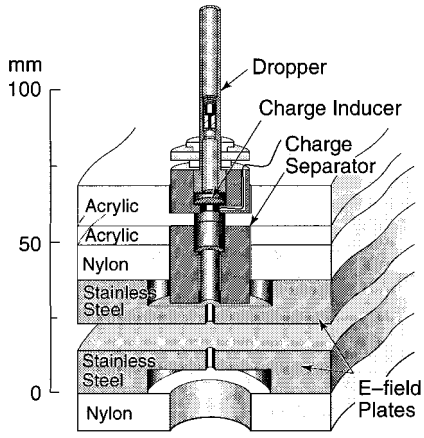

FIG. 3. Cross-sectional view of the entire dropper ensemble. The dropper is situated in a Delrin holder placed in a sheet of transparent acrylic that is attached to an x-y stage used to align the dropper to the charge separator. The second acrylic sheet holds the charge separator and is fastened to the nylon platforms. The electric-field plates are attached to the nylon platforms.

is necessary to prevent excessive surface wetting of the orifice and fluid leakage during the equilibrium state. Empirically, it has also been observed that a slightly negative manometer pressure gives us more reliable single drop production. (For a general introduction to drop-on-demand systems, see [9] and the references therein.)

B. Charge inducer mechanism and charge separator

The dropper is situated in a 2.5-cm-diam Delrin holder with a 0.28-mm-thick concentric steel charge inducer plate located parallel to the ejection orifice with a 1-mm separation (Fig. 3). The inducer plate has a 100-μm through hole. No electrical contact is made between the dropper, which is grounded, and the inducer plate, which is held at a positive or negative voltage, depending on whether we wanted to induce net positive or negative charge on the drops. However, because we preferred to work with neutral or close to neutral drops, the charge inducer was very rarely used.

The dropper and holder are placed inside a 2.5-cm hole in a 12.7-mm-thick sheet of transparent acrylic. The acrylic sheet is attached to an x-y stage used for aligning the dropper to the charge separator. The base of the x-y stage is mechanically connected to a 6.4-mm-thick sheet of transparent acrylic that has a 2.5-cm hole that holds the separator. The charge separator consists of two small, flat electrode plates about 0.25 mm thick, 8 mm wide, and 1.2 mm high inserted along two diametrically opposite grooves milled into a 3-cm-high Delrin rod. A transverse electric field is set up between the two electrodes. During the troubleshooting phase of the experiment, we used the charge separator to spatially separate the charged drops. A typical value of the magnitude of this field would be 2×10^4 V/m. The actual field, however, depended on the tests we were running. The charge separator was not used during data acquisition.

C. Electric-field plates

The stainless-steel electric-field plates are 15.24 cm in diameter and have 0.79-mm concentric holes through which

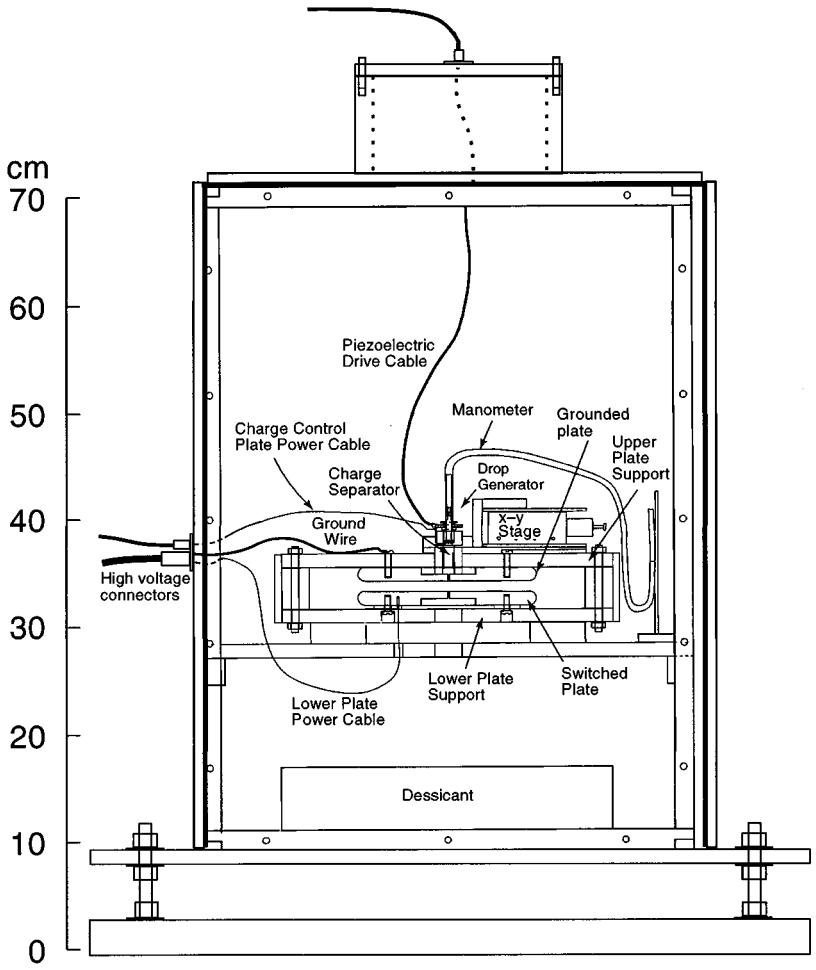

FIG. 4. Diagram of the experimental chamber.

the drops fall. The dropper, holder, and charge separator ensemble is placed in a 2.5-cm through hole in a 22.9×30.5 cm^2 nylon platform, which is attached to the top electric-field plate with screws. The bottom plate is likewise attached to a second nylon platform with the same dimensions as the first. In addition to attaching the electric-field plates to the nylon platforms, the screws have the added benefit of enabling us to adjust the parallelism of the plates. The two platforms are

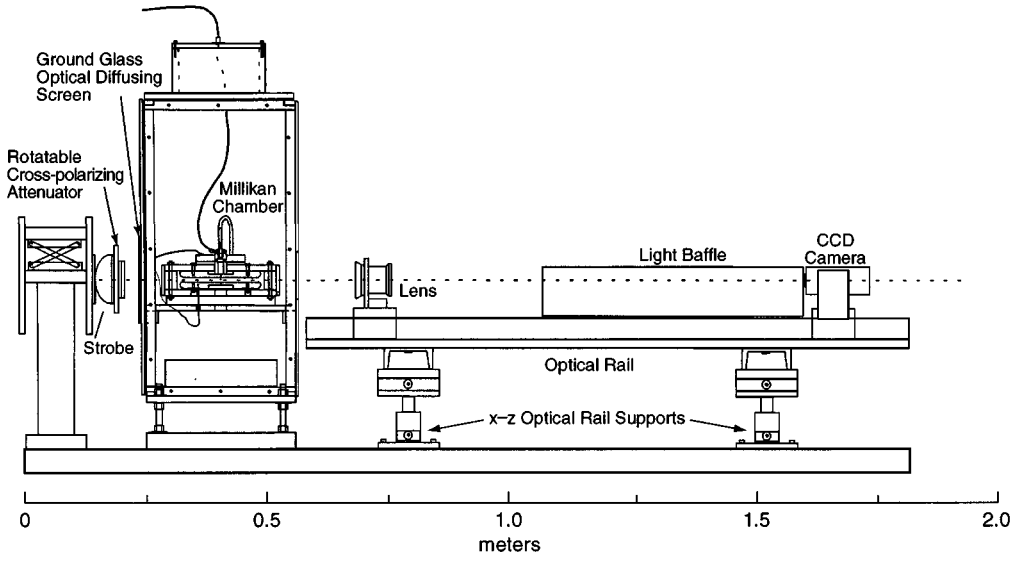

FIG. 5. Diagram of the experiment showing the stroboscopic source at the far left, the apparatus, the lens, and the CCD camera.

connected by pillars at the four corners. Since the drops used are 7.1 μm in diameter, they are extremely sensitive to air currents. Therefore, it is necessary to provide shielding against convection and other air currents by isolating the electric-field region. Thus the remaining four faces of the box are covered with 6.35-mm-thick transparent acrylic. This material was chosen so that we can illuminate and view the falling drops. The entire assembly is located within another chamber with 9.5-mm-thick transparent acrylic walls because we had observed that a single air current shielding box was insufficient (Fig. 4).

D. Drop velocity measurement method

The drops are backlit by a stroboscopic source [18] flashing at 9.99 Hz (Fig. 5). A 210-mm focal length lens, 30 cm away from the dropper, focuses the image of the drop's shadow as it falls between the two electric-field plates onto a CCD video camera 106 cm away from the lens. The RS-170 (US black and white television) analog signals from the CCD camera are converted to a digital image by a video capture card installed in a 90-MHz Pentium desktop computer. The data acquisition program analyzes the image and locates the position of the drop. Two captured images are required for one velocity measurement. The time between image captures is 100.1 ms. After one velocity measurement is completed, the electric field switches direction and two more images are captured for another velocity measurement. In this way multiple velocity measurements are made per drop. For every two velocity measurements, one charge calculation is generated according to Eq. (9).

Since our charge measurements are determined by measuring velocities, determining the time intervals between drop measurements and the position of the drops has to be performed with high precision. The clock pulses coming from the CCD camera are separated by 100.1001 ms with a variation of approximately 0.5 μs. The electric-field switching time was verified on an oscilloscope using an internal 1000:1 voltage divider. It was ascertained that the switching time was sufficiently short that the electric field is able to settle to its final value before the next measurement cycle begins. This switching time constant was measured to be approximately 4.7 ms. The precision of the position of the drops are discussed in the following sections.

E. Camera, image digitization card, and drop position precision

The drops are imaged with a standard RS-170 output commercial grade CCD video camera [19]. The active region of the CCD sensor is a rectangular region that is 6.4×4.8 mm^2, divided into 182 710 (755×242) pixels. The strobe flash illuminates the active region of the CCD camera for 4 μs and the entire active region is read out and encoded in each RS-170 field. The dimensions of a pixel are 8.5 μm along the 6.4 mm dimension and 19.5 μm along the 4.8-mm dimension. Within the 4.8 mm, there are 242 pixels; an internal pseudo-interlacing procedure involving intensity averaging over alternate vertical pixels generates the 484 scan lines required by the RS-170 video standard. The CCD chip uses full frame transfer technology that gives a theoretical 100% fill factor for the photosensitive regions. The camera is turned 90° from the usual orientation so that the 6.4 mm direction is parallel to the path of the falling drops. This gives higher measurement resolution and avoids the image position distortion caused by the internal pseudo interlacing procedure.

The optical system images from the drop plane to the camera focal plane with a magnification of about 4.0. Thus each CCD camera pixel images an area of 2.1 μm high by 4.9 μm wide in the real space of the falling drops. Recall that the drops are 7.1 μm in diameter. The rms vertical positional accuracy with which the drops could be located in the real space of the falling drops was less than $\sigma_z=0.35$ μm, which corresponds to 17% of the vertical pixel dimension.

The charges on the 755×242 CCD pixels are transmitted via RS-170 standard video signal, to a video image capture device, a monitor, and a video cassette recorder. This video image capture device is an ImageNation Cortex-I, 8-bit (256 gray scale) resolution, memory buffering image capture card. CCD imaging systems that do a direct transfer of digitized CCD image to computer memory are available, but are generally an order of magnitude more expensive than standard RS-170 analog output cameras.

Each horizontal video line (vertical real space) is digitized internally by the capture card into 512 memory mapped pixels representing 3.1 μm in real space in the image plane of the falling drops. Since RS-170 signals are internally dual interlaced and a strobed image produces illumination over only one of the two internally overlapping fields, the camera vertical line resolution (horizontal real space) is only 242 lines. This is not an important loss of data because the lateral velocities of the drops are near zero and are not used to determine the electric charge on the drops. The reduction of real-space vertical pixel resolution from the 755 CCD pixels per scan line to an internally represented 512 pixels also does not represent a significant loss in position information because the horizontal modulation transfer function of the camera goes to zero past the 550 horizontal lines due to electrical bandwidth limitations.

F. Drop position algorithm

The essence of the drop position algorithm is to repeatedly find the real-space position of a single drop image by computing the weighted centroid of the pixel intensities of the drop image. Since the drop is backlit, the shadow is darker than the background illumination, so the pixel gray scale values are inverted (i.e., 255 minus gray scale value) before weighing to ensure that the darker pixels receive more weight. Based on the available computational power, the algorithm design philosophy is to locate and track the position of a single drop image in a single pass of the image without performing detailed (and computationally intensive) image analysis and without storing any image data. In order to do this within 100 ms, the algorithm had to be simple and concise. However, the simplicity required of the algorithm to meet the 100 ms time budget introduced the possibility of false triggers due to multiple drop images in the same field of view. Therefore, it was necessary to add real time cuts to the data.

The algorithm consists of two steps: search and track. In the search step, no valid drop images were located in the previous frame and any previous track histories were written to disk and no longer available. Each subsequent frame is examined using a two-level trigger to locate a drop image in the frame. The first level searches the frame by examining every other pixel of every other row for any pixels that are darker than some threshold value. If at least one dark pixel is found, a coarse centroid of all dark pixels is passed to the second level trigger. If there are two or more drops, the centroid is computed with pixels from both. The ideal algorithm would compute the distances between various dark pixels so that clusters can be detected and multiple coarse centroids computed. In practice, however, such an algorithm proved to be too computationally intensive to use in a real time search.

Since the algorithm is designed to measure the charge of only one drop at a time, the second level trigger was designed to eliminate the case where two drops are in the field of view at the same time or there was sufficient nonuniformity in background illumination to cause one or more background pixels to fall below the threshold. However, as discussed in Sec. V B 1, double drops still posed a problem. Using the coarse centroid of dark pixels passed from the first level trigger, the second level trigger examines the 11×11 pixel subframe centered on the coarse centroid. In a single pass, it computes an average of the four corner pixels to determine the level of the background illumination, sorts the remaining 117 pixels, and computes a refined centroid using only the 20 darkest pixels after subtracting the mean background illumination. If the mean weight per pixel of the 20 darkest pixels (assumed to be part of the drop image) is more than 2 below the mean background, then the trigger passes the refined centroid to the tracking routine as a valid drop position.

If the first level falsely triggers on random fluctuations in the background illumination, the second level trigger should reject the event since the rms fluctuation of the background illumination has consistently been observed to be less than two levels of gray scale from the mean value when averaged over an 11×11 subframe. If the first level triggers on two drop images in the field of view, then, if the drop centroids are separated by more than 50 μm in real space and are of equivalent darkness, the coarse centroid will fall in the region between the drops. If the drops are much closer, then the second level trigger will pass this detection as a valid drop, leaving the final rejection to the tracking algorithm.

The tracking algorithm uses the same two-level trigger as the search algorithm and maintains a stack of at most four drop positions at any given time, since this is all that is required for a single charge measurement. When a track has been started and a frame fails to pass the search trigger, all track data are written to disk and the algorithm returns to search mode. Additionally, if there is a drop image that was near the bottom of the field of view in one frame and there is another image near the top of the field of view in the next frame, the tracker assumes that one drop exited and a new one entered and writes all past track data to disk and starts a new track.

Two positions are recorded for each orientation of the field to determine $v_{E_{\mathrm{up}}}$ and $v_{E_{\mathrm{down}}}$. If the drop moves in a direction opposite the field orientation, then the velocity is signed negative. The horizontal velocities are also calculated and used to reject drop trajectories that have a sudden increase in horizontal velocity. This is the first cut on a multiple drop event, since a heavy, fast-moving drop may overtake a slower drop for one or two frames, which pulls the centroid to one side and causes a large horizontal velocity. When one velocity for each field orientation is measured, the tracker computes the charge. We can see from Eq. (9) that it might be possible to compute an imaginary result. Physically, this can never happen, so this becomes the second cut on multidrop events.

IV. DEVELOPMENT OF EXPERIMENT, OPERATION OF EXPERIMENT, AND DATA

A. Development of the experiment

Our goal in the experiment was to search for isolated fractional electric charge in about 1 mg of Dow-Corning 200, 5-cS (1 cS$\equiv10^{-2}$ cm^2/s) silicone oil. In the beginning of the experiment, we knew that we required drops with diameters of 10 μm or less to obtain sufficiently good charge measurement precision. However, there were many questions that could only be answered by experimentation. Among these were: How uniform would be the drop size? At what rate could we make the drops? What drop size would give the best precision? How rapidly could a PC-type desktop computer with a video image capture board determine and record the drop charge in real time?

Therefore, when we began operating the experiment, we mixed periods of data acquisition with periods of apparatus testing, apparatus improvement, computer program improvement, and troubleshooting. Two months later we were able to devote most of the experimental time to data acquisition. The experiment had to be interrupted for about two months when a five-month-long renovation of the roof and air-conditioning system of the building forced us to move the apparatus to a seismically quieter location. The experiment was resumed, and then ended two months later, seven months after initiation.

During the entire experiment, we saved the position-time trajectory measurements of every drop produced during a data acquisition run on the hard drive of the acquisition computer. When the hard drive reached maximum capacity, we transferred all the data for all the runs on the hard drive to back-up data cartridges and then proceeded to purge the hard drive.

In the early stages of the experiment, we found that the precision of the drop charge measurement improved as the drop diameter decreased. The principal reason is that smaller drops have smaller gravitational terminal velocities, as shown in the equation

$$v_{g,\mathrm{terminal}}=\frac{2r^2(\rho_{\mathrm{oil}}-\rho_{\mathrm{air}})g}{9\eta}. \tag{10}$$

Drop charge measurement precision improves as the ratio $v_{E,\mathrm{terminal}}/v_{g,\mathrm{terminal}}$ increases, $v_{E,\mathrm{terminal}}$ being the component of velocity produced by the QE force [Eqs. (2) and (3)]. On the other hand, since the goal of the experiment was set at 1 mg total of drop masses, the smaller the drop, the larger the

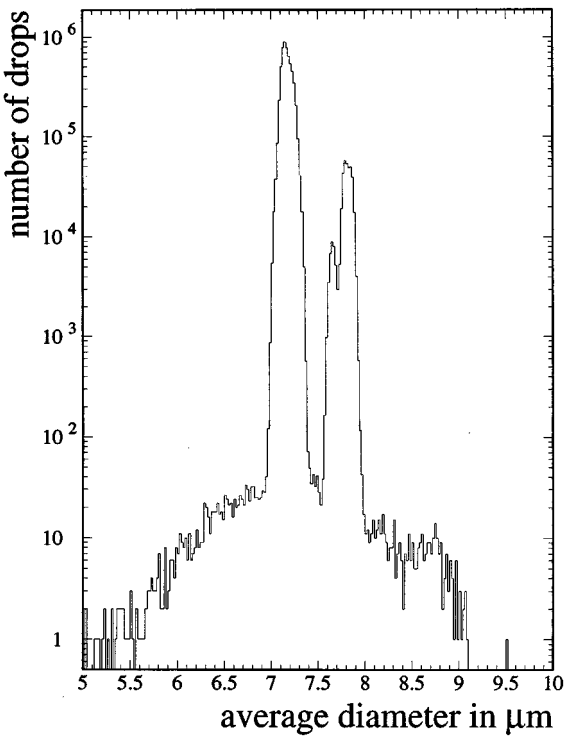

FIG. 6. Histogram of the average diameter of the drops produced. The initial stage of data acquisition utilized 7.6 μm drops. The remainder of the experiment used 7.1 μm drops.

number of drops that must be studied. We compromised with a drop diameter of 7.1 μm. Figure 6 shows the size uniformity of the drops produced.

We found that two factors placed an upper limit on the rate at which drops could be generated and their charge measured. First, the algorithm for finding the drop position failed if the image captured more than one drop (Sec. III E). Second, for reasons we did not understand, as the drop generation rate increased above 1 Hz, drop production became irregular until two or more drops are produced simultaneously. This led to unreliable data, as discussed in Sec. V. Therefore, for clean, consistent data we set the drop generation at 0.6 Hz. As discussed in Sec. VII, our goal for the next experiment is to considerably increase the drop generation rate. Since the end of the experiment, we have found a way to operate the dropper with a frequency greater than 100 Hz.

The drop position detection algorithm was also determined to be sensitive to nonuniformity in the light field illumination. By affixing a ground glass screen on the side of the experimental chamber facing the strobe, we were able to diffuse the light from the stroboscopic source and thereby improve the uniformity of the light field illumination (see Fig. 5). We also found that the light distribution from the stroboscope changed slightly as the bulb aged. Therefore, we periodically readjusted the bulb position slightly and we replaced it once.

As the experiment went along, a phenomenon occurred and recurred that we do not yet understand. As already mentioned above, except for the first stage of operation, we did not attempt to induce any charge on the drop, the charge induction voltage was set to zero. Then most of the drops had zero charge with a few drops having charge $\pm 1e$ and rarely $\pm 2e$. After a few months of operation we noticed the charge distribution spreading to $\pm 3e$, $\pm 4e$, and even $\pm 5e$ with fewer drops having zero charge. We preferred to have $0e$, $\pm 1e$, or $\pm 2e$ because the precision of the charge measurement is better when the drop charge is small (see Appendix B) and a large spread leads to more drop measurements not meeting the criteria outlined in Sec. V B. The only way we found to reduce the charge distribution spread was to remove the old oil in the dropper and fill the dropper with new oil, the new oil being taken from the same storage container as the old oil. Then over a period of several months, the limits of the charge distribution once again spread from $\pm 2e$ to $\pm 5e$. Our speculation is that ions form in the oil either due to chemical interaction of the oil with the dropper material or due to diffusion of contaminants that appear because the manometer is open to the atmosphere. We have no evidence for this speculation.

B. Operation of the experiment

During periods of data acquisition, we operated the experiment continuously, 24 h per day and 7 days per week. Table I illustrates the data and calculations recorded for each drop on the computer hard disk. The data acquisition was divided into runs about 9 h long, each run containing about

TABLE I. Sample of data taken for a typical drop. The drop is identified by a tag number shown in the first column. The field direction is given by the polarity. A polarity of -1 indicates that the electric field is pointing down and a polarity of $+1$ indicates that the field is pointing up. The values under the columns entitled Row_1, Column_1, Row_2, and Column_2 locate the centroid of the drop in terms of pixels at two different times separated by 100.1 ms. (The pixel positions are recorded to three decimal places for conveniences in performing calculations, but the measurement precision is about one decimal place.) The horizontal velocities of the drop shown in the column entitled v_x and the vertical velocities of the drop are given in the adjacent column, both in mm/s. The last column shows the net charge on the drop.

Drop. No.	Polarity	Row_1	Column_1	Row_2	Column_2	v_x	v	Q/e
1	-1	180.971	38.341	181.366	84.301	0.0093	1.3830	
1	$+1$	181.696	129.739	181.972	174.972	0.0065	1.3611	0.0605
1	-1	182.710	220.573	183.127	266.399	0.0098	1.3789	0.0493
1	$+1$	183.432	311.861	183.499	357.009	0.0016	1.3585	0.0564
1	-1	184.369	402.686	184.353	447.772	-0.0004	1.3566	-0.0052

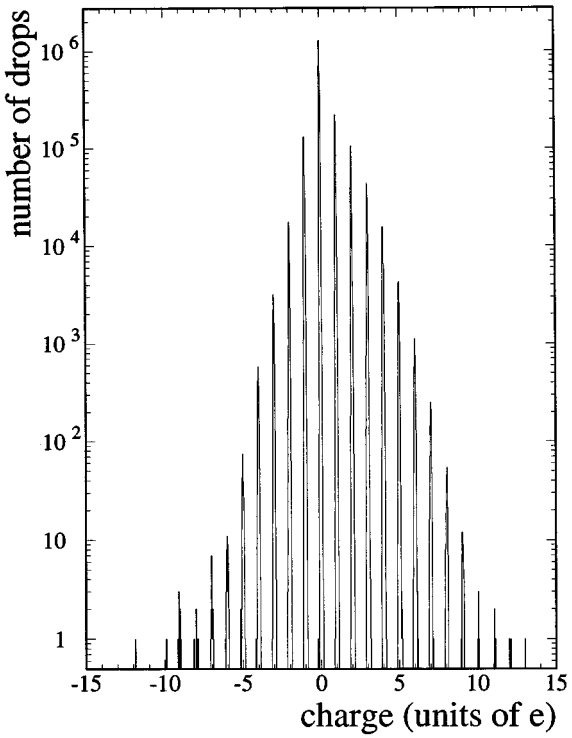

FIG. 7. Histogram showing the distribution of the charge on the 5 974 941 accepted drops. Note that a majority of the drops are neutral or are close to neutral.

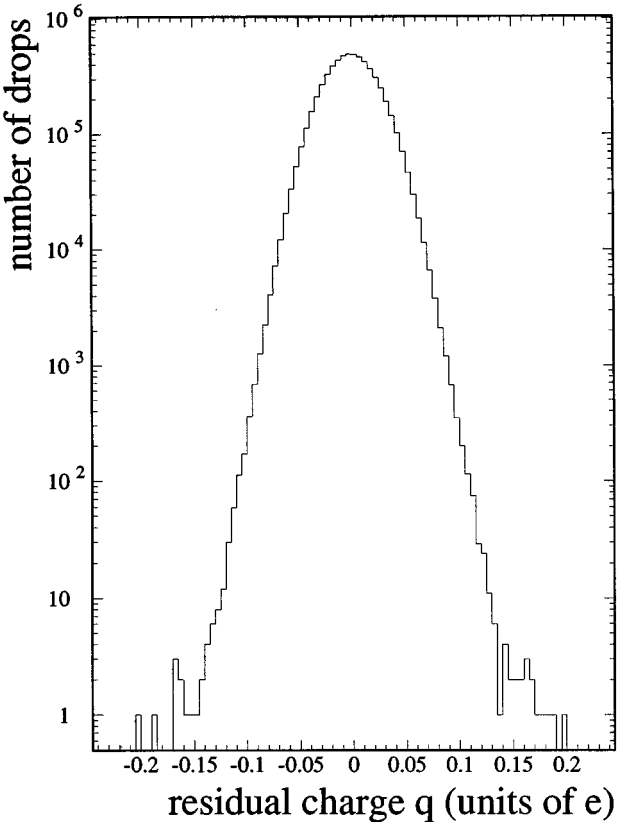

FIG. 8. Histogram showing the residual charge on the 5 974 941 drops. The residual charge is defined by $q=Q/e-N_c$. A Gaussian fit yields $\sigma_q=0.025$.

10 Mb of data. The data from each run was put through a data analysis program to look for any free fractional electric charges and to make sure the apparatus was working properly. If the data showed unusual properties, such as an abnormally high drop rejection rate, data acquisition was stopped until a solution was found. When about 600 Mb accumulated on the hard disk, the data were transferred to a back-up data cartridge.

C. Data

During the course of the experiment, we measured the charge on 6 161 651 drops. Using the criteria for acceptance of drop charge measurement discussed in Sec. V B, there are 5 974 941 drops in the accepted charge measurement category. Thus approximately 3% of the drops were rejected. These drops have a total mass of 1.07 mg and comprise a total of 6.41×10^{20} nucleons.

V. MEASUREMENT OF DROP CHARGE: EXPERIMENTAL PRECISION, CRITERIA FOR ACCEPTED CHARGE MEASUREMENTS, AND LIMITATIONS ON PRECISION

A. Presentation of data

Figure 7 is a histogram of the accepted charge measurements for the 5 974 941 accepted drops. The distribution shows that most drops have a charge Q in the range between $\pm5e$ with the $0e$ peak dominant. As discussed in Appendix B, neutral drops led to slightly higher precision charge measurements.

In analyzing the data, we define N_c as the signed integer closest to Q/e. Then

$$q=\frac{Q}{e}-N_c \tag{11}$$

is the signed deviation of the measured charge from the closest integer charge. Figure 8 is a histogram of q for the entire experiment. This histogram is approximated by a Gaussian distribution with

$$\sigma_q=0.025. \tag{12}$$

This fit has a χ^2 per degree of freedom of about 1.5. This is the experimental precision of the drop charge measurement. We are pleased with this small σ_q. In Sec. V C we discuss the factors that may be preventing an even smaller σ_q.

Figure 9 is another presentation of the data shown in Fig. 8. We define N_s as the largest non-negative integer less than $|Q|/e$ and then define

$$q_s=\frac{|Q|}{e}-N_s. \tag{13}$$

This is the histogram that we use to search for fractional charge, hence subscript s for search. Figure 9 also shows the search range to which q_s is sensitive. During the experiment we looked at the data as they were produced in the presentation of Fig. 9. Our provisional criterion for possible fractional charge events was that

$$0.2<q_s<0.8. \tag{14}$$

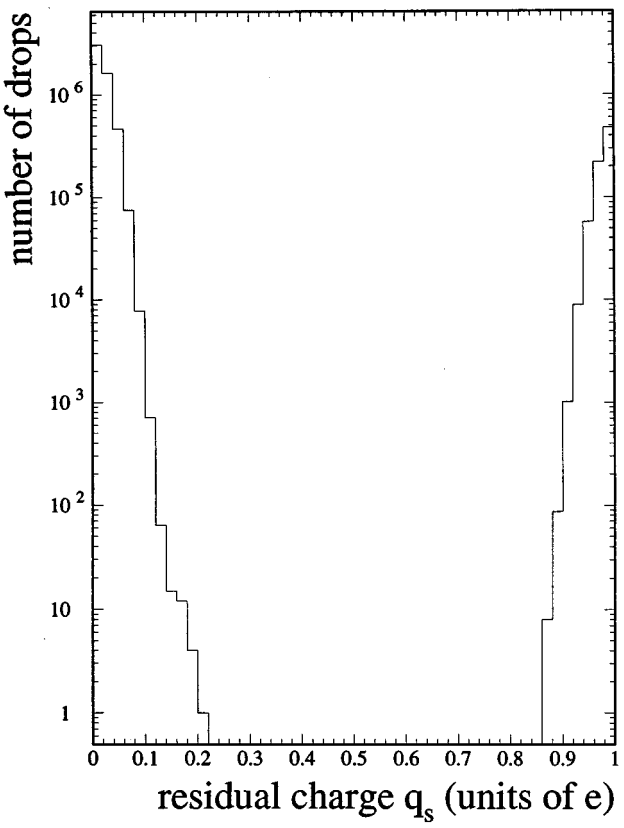

FIG. 9. Another representation of the data presented in Fig. 8 showing the residual charge. Here residual charge is defined by $q_s=|Q|/e-N_s$. Histograms of this type were viewed for the individual runs to look for anomalous events. As shown above, no fractionally charged particles were found.

Such a drop would have a charge differing by more than eight standard deviations from an integer charge and its charge should be measured with the same precision as the other drops. From Fig. 9 we see that there are no fractionally charged particles with a charge of $\pm\frac{1}{3}e$ or $\pm\frac{2}{3}e$. We note that there is one event that shows an absolute charge greater than $0.2e$. The charge on that one drop was $-0.2045e$. Therefore, that event is merely part of the tail. (We also note at this point that fractionally charged particles with measured charge within $0.2e$ of integer charge is indistinguishable from our measurement spread unless a significantly large peak were found that rose above the tail.) The final criteria for the fractional charge search are discussed in Sec. V B.

B. Criteria for acceptance of a drop charge measurement

As discussed in Sec. II, the determination of the charge and radius of a drop requires two velocity measurements $v_{E_{\rm up}}$ and $v_{E_{\rm down}}$. The first velocity measurement requires two vertical position measurements z_a and z_b; the second velocity measurement likewise requires two vertical position measurements z_c and z_d. If the charge on the drop changes at any position between z_a and z_d, a false fractional charge would be measured. The charge would change if a free ion or electron attaches itself to the drop or if the drop is hit by a cosmic ray. Therefore, a single measurement of the charge on a drop cannot be used for a fractional charge search.

Two measurements of charge, Q_1 and Q_2, on a given drop would allow a test for charge change by considering the difference $\Delta Q=Q_2-Q_1$. However, we felt more confident with requiring at least three measurements of charge per drop as it falls between the electric-field plates. This criterion of at least three charge measurements requires at least four different velocity measurements, which, in turn, require at least eight different position measurements along the trajectory of the drop. This means that the first and the third measurement of charge on a given drop are completely independent. Thus the first criterion of an acceptable drop charge measurement is

$$\text{criterion 1: 3 or more charge measurements.} \quad (15)$$

We use the arithmetic average

$$Q=\frac{Q_1+\cdots+Q_n}{n} \quad \text{where } n=3,\ 4,\ \text{or } 5 \quad (16)$$

to define the charge Q on the drop. To eliminate measurements that contain a charge change we define

$$Q_{\rm min}=\min(Q_1,\ldots,Q_n), \quad (17)$$

$$Q_{\rm max}=\max(Q_1,\ldots,Q_n), \quad (18)$$

$$\Delta Q=Q_{\rm max}-Q_{\rm min}. \quad (19)$$

We then require

$$\text{criterion 2:} \quad \Delta Q<\Delta_{\rm crit} \quad (20)$$

for the charge measurement on a drop to be called acceptable. The majority of all drops, 87.7%, have four charge measurements, 5.9% have three, and 6.4% have five. Our final choice for $\Delta_{\rm crit}$ is outlined in the following subsection.

These two criteria were originally developed to eliminate drop charge measurements that contained a charge change, but they turned out to be crucial in the elimination of two instrumentation effects. The first instrumentation effect is that the drop position algorithm depends upon uniform light field illumination of the falling drop. This uniformity was checked frequently by the experimenters and adjusted when necessary, but these adjustments had to be done by hand. Furthermore, the performance of the stroboscope bulb deteriorated with age and was affected by the line voltage of the building. We found that deviations from illumination uniformity could interfere with precise Q measurement by introducing noise in the target window. This noise appears as darkened pixels that would be taken by the drop finding algorithm as part of the drop centroid it is locating. This would give an erroneous position of the drop and therefore an erroneous charge measurement.

The second instrumentation effect eliminated by the two criteria is the inability of the drop finding algorithm to analyze events with more than one drop per video frame. Multiple drops might appear in a frame for two reasons. First the dropper occasionally produced two drops simultaneously. Second, drops produced at the rate of 0.6 Hz might occasionally appear in the same frame. As an illustrative example,

consider two drops, one positively charged and the other neutral. Assume that the neutral drop emerges from the dropper first. The positively charged drop then is initially only 1.67 s behind. But before either drop enters the active imaging area, they are affected by the electric field leaking through the 0.79 mm hole in the upper electric-field plate. The electric field always starts negative and field switching begins only after a drop enters the measurement region. Therefore, a drop experiences a negative field on average. The negative electric field leaking through this hole will accelerate the positively charged drop so that the spacing between the neutral drop and the positive drop will be diminished. Both drops reach terminal velocity, however, before they enter the measurement region of the electric field and on average the charged drop falls with the same velocity as the neutral drop during the time of measurement taking; therefore, the diminished spacing between the drops remains and they may appear in the same video frame.

1. Determining the final value for Δ_{crit}

As a preliminary analysis of the data, we considered in detail all drops for which

$$0.2<q_s<0.8 \tag{21}$$

and

$$\Delta Q<0.4e. \tag{22}$$

We called such drops anomalous.

At first we simply looked at the three separate charge calculations and the velocities from which the charges are derived. Then about one-third of the way through the experiment, we began to record on cassette tape the video image of the falling drops. We then looked back after each run at the video image of the anomalous drops if there were any. Initially we videotaped 16 h per day, eventually going to 24 h per day when the videotaping system was upgraded. Taking into account that our videotaping was incomplete, as just explained, we found that about 43% of the anomalous drops videotaped actually consisted of two close together drops. Such a configuration leads to errors in the calculation of the drop position because the centroid found by the drop finding algorithm is not the true centroid of either drop. We visually inspected over 10^3 drop images wherein the drops had

$$0.0<q_s<0.2 \quad \text{or} \quad 0.8<q_s<1.0,$$

and none of the viewed drops showed a double drop in the video image.

Returning to the anomalous drops defined by Eqs. (21) and (22), we found a total of 31 drops divided as follows: 10 drops, no video image; 12 drops, video images show 1 drop per image; 9 drops, video images show 2 drops per image.

As we mentioned earlier, we used the inequality $\Delta Q<\Delta_{\text{crit}}$ as a criterion to reject charge measurements in which there has been a charge change during the measurement and we used $\Delta_{\text{crit}}=0.4e$ during the data acquisition period in order to study the tails of the ΔQ distribution. However, approximately 97% of all charge measurements have $\Delta Q<0.15e$ (Fig. 10). Since we expect that the ΔQ distribution will be the same for drops with noninteger charge as for drops with integer charge, our final ΔQ acceptance criterion is

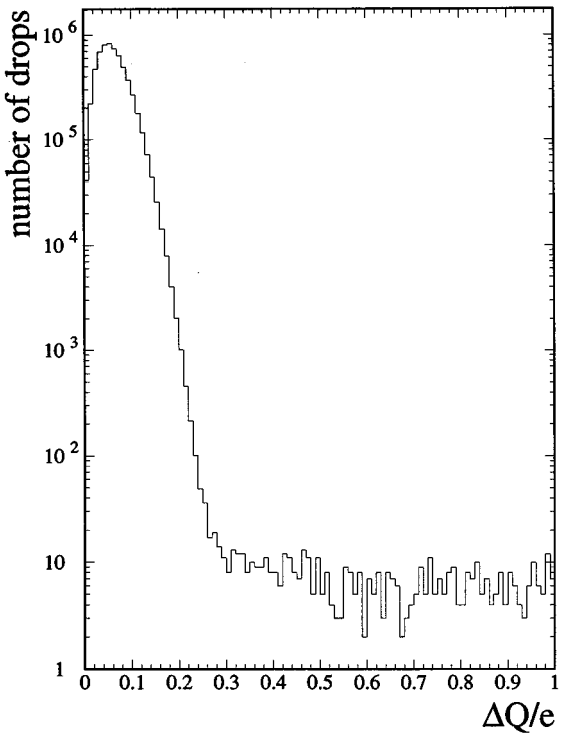

FIG. 10. Histogram showing that about 97% of the data have $\Delta Q<0.15e$. From the tail of the distribution we calculate that the upper limit to the number of drops that undergo a charge change during measurement is less than 0.02%.

$$\Delta Q<0.15e. \tag{23}$$

Our final criteria for noninteger charge events are then

$$0.2<q_s<0.8, \quad \Delta Q<0.15e. \tag{24}$$

These are the criteria for the data shown in Fig. 9.

C. Limitations on the precision of charge measurement

We have considered, and where possible, calculated or measured, the following phenomena, which may limit the precision of the drop charge measurement: (i) Brownian motion of the drop in air, (ii) change in mass of the drop by evaporation during fall, (iii) force on the drop due to the induced dipole moment, (iv) precision of drop position measurement, (v) apparatus vibration, (vi) air currents in the Millikan chamber, (vii) nonuniformity of the electric field, and (viii) time variation of the temperature in the Millikan chamber.

1. Brownian motion of the drop in air

The impact of air molecules colliding with the drop causes a fluctuation in the vertical velocity of the drop given by

$$v_{\text{Brownian}}=\sqrt{\frac{kT}{m}}, \tag{25}$$

where T is the air temperature and m is the mass of the drop. This leads to

$$\sigma_{q,\text{Brownian}}=0.021, \tag{26}$$

the square of which is about 70% of the measured precision of σ_q^2. For a fixed drop mass m, $\sigma_{q,\text{Brownian}}$ is the lower limit on the attainable charge measurement precision. Appendix A gives a detailed derivation of this value.

2. Change in drop mass due to evaporation

Another factor that contributes to σ_q is the evaporation of the drop as it falls. The change in the mass of the drop has an effect on the charge measurement because a mass change causes a velocity change and therefore an apparent charge change, Eq. (9). In the initial stages of the Millikan oil drop experiment, we actually started with water as our test fluid. However, evaporation of the water drops was not a problem we could overcome to our satisfaction [20]. To test whether the Dow Corning fluids also demonstrated a high evaporation rate, we conducted bulk studies of the 5 cS silicone oil and empirically compared its evaporation rate with those of the 1 and 2 cS fluids. Although the bulk studies showed negligible evaporation, evaporation is, in fact, observable in our experiment because of the small drop size.

We measured the average value $(\partial v/\partial z)_{\text{evaporation}}$ by taking a run with the electric field off, that is, with zero electric field, and for each drop, considering the four or more sequential velocity measurements: $v_a, v_b, v_c, v_d, \ldots$. Let z_a be the average position during the determination of v_a and so forth. We then calculate $(\partial v/\partial z)_{\text{evaporation}}$ by averaging over the quantities $(v_b-v_a)/(z_b-z_a)$, $(v_d-v_c)/(z_d-z_c)$,. . . and over all the drops. We find

$$(\partial v/\partial z)_{\text{evaporation}}=-3.03\times10^{-6}\quad \text{mm/s } \mu\text{m}. \tag{27}$$

Therefore, over one charge measurement cycle wherein the drop traverses approximately 287 μm, this velocity gradient leads to an error in the velocity measurement of 8.75×10^{-4} mm/s. This provides an upper limit to the average error in q of

$$\delta_{q,\text{evaporation}}=2\times10^{-3}. \tag{28}$$

However, evaporation affects all drops similarly and presumably this error does not fluctuate from measurement to measurement and is taken into account in the calibration (see Sec. V D). Any errors arising from evaporation is therefore negligible in comparison to $\sigma_q=0.025$.

3. Force on drop due to induced dipole moment

The vertical electric field of 1.4×10^6 V/m induces an electric dipole moment in the drop. If the electric field were spatially uniform, that is, $E_z=$const, there would be no net force on the drop due to the induced dipole, but the holes in the centers of the electric-field plates break the uniformity. Along the vertical symmetry axis of the plates, the field is smaller near the holes and has a maximum halfway between the plates. Therefore, $\partial E_z/\partial z$ is not zero and the interaction of the induced dipole with $\partial E_z/\partial z$ produces a dipole force on the drop proportional to $\partial E_z/\partial z$. By Stokes' law, this dipole force changes the terminal velocity by an amount v_{dipole} that is proportional to the dipole force. We denote by $v_{g,E}$ the terminal velocity of the drop caused by the gravitational and electric force so that the total velocity of a drop is given by $v=v_{g,E}+v_{\text{dipole}}$. Both $v_{g,E}$ and v_{dipole} are given a positive sign when they are in the downward vertical direction. Near the top plate, $v_{\text{dipole}}(\text{top})$ is positive, that is, downward and

$$v=v_{g,E}+v_{\text{dipole}}(\text{top})>v_{g,E}. \tag{29}$$

As the drop continues to travel, v_{dipole} decreases in magnitude but remains directionally the same. At the center, the velocity of the drop is given by

$$v=v_{g,E} \tag{30}$$

since $v_{\text{dipole}}(\text{center})=0$. When the drop passes the center, v_{dipole} changes direction and is then upward. Therefore, $v_{\text{dipole}}(\text{bottom})<0$ and

$$v=v_{g,E}+v_{\text{dipole}}(\text{bottom})<v_{g,E}. \tag{31}$$

Thus the field nonuniformity then has the overall effect of monotonically reducing v as the drop falls, giving a nonzero $\partial v/\partial z$. However, we make our measurements in the central 1.6 mm between the electric-field plates where $\partial v/\partial z$ is negligible (see Sec. V C 7).

Using a method similar to the one described in Sec. V C 2 for finding $(\partial v/\partial z)_{\text{evaporation}}$, we measured the average value $(\partial v/\partial z)_{\text{dipole}}$ by taking a typical run and selecting the charge zero drops. Again, for each drop, we considered the four or more sequential velocity measurements: $v_a, v_b, v_c, v_d, \ldots$ and calculated $(\partial v/\partial z)_{\text{dipole}}$ by averaging over the quantities $(v_b-v_a)/(z_b-z_a)$, $(v_d-v_c)/(z_d-z_c)$,. . . and over all the drops. Subtracting the effect due to evaporation, we find

$$(\partial v/\partial z)_{\text{dipole}}=1.73\times10^{-6}\ \text{mm/s } \mu\text{m}. \tag{32}$$

Again, over one charge measurement cycle, this leads to an average error in q of

$$\delta_{q,\text{dipole}}=1\times10^{-3}. \tag{33}$$

Compared with $\sigma_q=0.025$, $\delta_{q,\text{dipole}}$ is negligible.

4. Precision of drop position measurement

There is a lower limit set on the precision with which the z position of a drop can be measured, the limit arising from the nonzero size of the CCD pixel and defects in the drop position algorithm. We have not found a way to measure this precision. All we can do is find an upper limit on σ_z by assuming that the major components of σ_q are $\sigma_{q,\text{Brownian}}$ and σ_z. Then we find

$$\sigma_z\leqslant0.35\ \ \mu\text{m} \tag{34}$$

in real space, which is 17% of a pixel.

5. Apparatus vibration

When we began the experiment, we found that some part of the initial σ_q was caused by vibrations of parts of the apparatus. These vibrations, in turn, arise from the vibrations

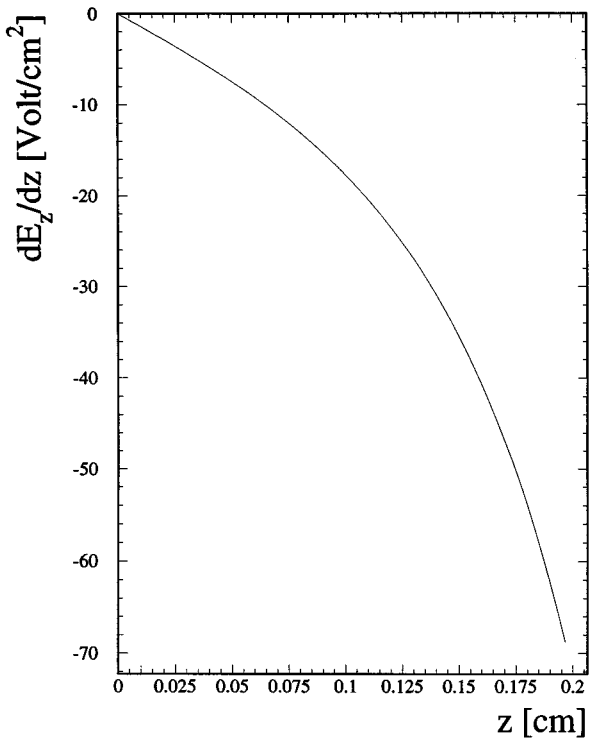

FIG. 11. Numerical calculation of the gradient of the electric field. Halfway between the plates, z is zero.

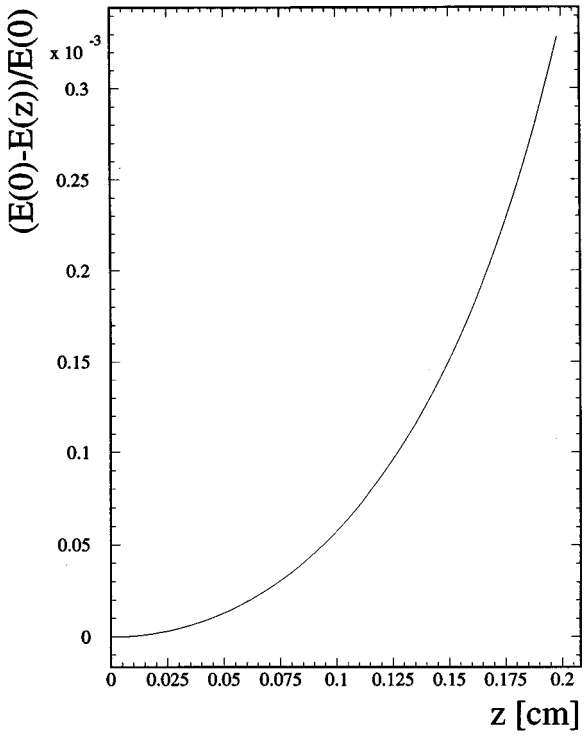

FIG. 12. Numerical calculation of the electric field. Shown is the relative deviation of the z component of the electric field from its value at the center between the plates.

in the walls and floor of the building. Therefore, the apparatus was built on a wooden table that was stiffened with two I beams. Weights were placed on the table to further dampen residual resonances. We also moved the entire assembly to that part of our laboratory room with the smallest wall and floor vibrations. The effect of residual vibrations on σ_q is included in σ_z.

6. Air currents in the Millikan chamber

We have eliminated observable air currents in the Millikan chamber by enclosing the chamber in double walls and by operating the experiment in a temperature controlled room. Unobservable air currents may contribute to σ_q since

$$v_{\text{measured}} = v_{g,E} + v_{z,\text{air}}, \tag{35}$$

where $v_{z,\text{air}}$ is the z component of the air velocity. We have not found a method to measure $v_{z,\text{air}}$. We can, however, set an upper limit on the average horizontal component of the air velocity $v_{x,\text{air}}$ by looking at the measurements of the horizontal position of a drop as it falls. By taking the root mean square of the lateral velocities of each drop and then taking the root mean square of that value, we obtain

$$|v_{x,\text{air}}| \leq 0.013 \ \text{mm/s}. \tag{36}$$

Of course, $v_{z,\text{air}}$ can easily be larger. Therefore, $v_{z,\text{air}}$ may contribute to σ_q.

7. Nonuniform electric field

Figure 11 shows a numerical calculation of $\partial_z E_z$ along the z axis. The calculation used a computer relaxation method that generates the value of the electric field by calculating the charge distribution on the plates.

As mentioned earlier, E_z is smaller at the plates because of the holes in the plates. The variation in the center region is very small. We use the central 1.6 mm of the vertical distance for viewing the drops, thus taking measurements where E_z is most uniform. The calculation shows that

$$\frac{E_z(0) - E_z(z)}{E_z(0)} \sim 10^{-4} \tag{37}$$

in the region of interest (Fig. 12). The charge measurement is affected by the same negligible factor.

The same calculation also provides an estimate of the dipole force, which is given by

$$F_{\text{dipole}} = P_z \frac{\partial E_z}{\partial z}, \tag{38}$$

where P_z is the z component of the induced dipole moment on the drop

$$P_z = 4\pi\epsilon_0 \frac{\epsilon - 1}{\epsilon + 2} r^3 E_z. \tag{39}$$

For silicone oil $\epsilon \sim 2.7$ [21], which implies $P_z = 1.46e$ cm. The gradient $\partial_z E_z$ in the central region varies from about -11 to 11 V/cm^2, which leads to variations in the apparent charge of about $\pm 1.2 \times 10^{-3} e$. Since this is the maximum variation, this result is in good agreement with the experimentally observed fluctuation of $\pm 1 \times 10^{-3} e$.

8. Time variation of temperature in Millikan chamber

As previously discussed, to minimize the effects of temperature on the data, the experiment is conducted in a temperature controlled room and thermometers in the measurement chamber enable us to enter temperature as a parameter in our data acquisition program. As yet, however, the instantaneous temperature is not directly supplied to the charge calculation code in the computer and must be entered manually. We have observed temperature fluctuations of up ± 2.5 °C per day.

The temperature dependence of the charge [Eq. (9)] comes in two places, the viscosity and density of air. The correction arising from the latter is small compared with that from the viscosity of air. A ± 2.5 °C change in temperature causes a variation in the viscosity of air of $\pm 0.65\%$. This in turn leads to a variation of the calculated drop charge of

$$|\delta_{q,\mathrm{temp}}| \leqslant 0.01. \tag{40}$$

This may be an important contribution to $\sigma_q = 0.025$. We regret that we did not directly supply the instantaneous temperature of the Millikan chamber to the charge calculation code. Our analysis is based on an average temperature of 22.0 °C.

D. Calibration

We conclude this section with a short discussion on the limitations of the absolute charge measurement. Since the goal of this experiment was to detect fractional charges, great care has been taken to eliminate fluctuations in individual charge measurements. However, there was no need to optimize the accuracy of the absolute measurement. Instead the integer spacing of the drop charges has been used to calibrate the measurement apparatus and has been absorbed into the empirically determined magnification factor of the optical system. This magnification had to be readjusted only when the oil was changed (because this necessitated removing the dropper from the system and then replacing it) and can absorb an overall adjustment of about 3%. As a consequence, it was not necessary to include corrections for the slight nonsphericity of the drops due to air drag and interaction with the electric field, nor have we included the small radius corrections to Stokes' law that Millikan applied. For the drop size considered here, these effects are very small and since they affect all drops equally, they are simply absorbed in the calibration.

VI. CONCLUSION

As shown in Fig. 9, once the measured charge is within $0.2e$ of integer charge and the measured charge approaches that integer, the sensitivity of search rapidly decreases. Therefore, our main conclusions are for charges that are at least $0.2e$ distant from an integer charge: namely, the regions

$$0.2e \text{ to } 0.8e,\ 1.2e \text{ to } 1.8e,\ 2.2e \text{ to } 2.8e,\ldots,$$

$$-0.2e \text{ to } -0.8e,\ -1.2e \text{ to } -1.8e,$$

$$-2.2e \text{ to } -2.8e,\ldots .$$

TABLE II. Limits obtained in bulk matter searches.

Group	Material	Mass (mg)
LaRue *et al.* [12]	niobium	1.1
Marinelli *et al.* [13]	iron	3.7
Liebowitz *et al.* [14]	iron	0.72
Smith *et al.* [15]	niobium	4.87
Milner *et al.* [17]	niobium/tungsten	
Joyce *et al.* [2]	sea water	0.05
Savage *et al.* [4]	native mercury	2.0
This experiment	silicone oil	1.07

In 1.07 mg of silicone oil we have not found any accepted drops with fractional charges in these regions. This 1.07 mg contains 6.41×10^{20} nucleons. Therefore, with 95% confidence the concentration of particles with charges in these charge regions in silicone oil is less than one per 2.14×10^{20} nucleons. This result, of course, applies to the specific case of searches for isolated quarks with the charge taken to be $\pm 1/3e$ or $\pm 2/3e$.

Table II lists the results of other published searches for isolated quarks with charge $\pm 1/3e$ or $\pm 2/3e$. Ignoring the differences in the material examined, we see that our null result agrees with the null results found by all the experiments except LaRue, Phillips, and Fairbank [12]. These null experiments range from being about 5 times more sensitive than our search to being about $\frac{1}{20}$ as sensitive. Our experiment uses an organic material, but we do not consider this important.

We have developed a reliable method of searching for fractional electric charge in bulk material. As discussed in the next section, we know how to greatly increase the rate at which we produce and examine drops. Therefore, we know how to examine samples up to 100 mg in mass, ultimately perhaps 1000 mg. Also, while oil is the most convenient material for our present experiments, we believe that our method can be extended not only to other liquids, but to suspensions of small particulates in liquids.

VII. PROPOSED IMPROVEMENTS AND FUTURE EXTENSIONS

The goal of our next experiment is to increase, by at least a factor of 100, the rate at which we produce drops and measure their charges. While the charge measurement precision and the reliability of the experiment are adequate, some improvements are required. The computer system, including the video digitization card, must be able to find drop positions, calculate drop velocities, calculate drop charge and mass, and record at a rate greater than 10 Hz and eventually up to 100 Hz. The algorithms for finding drop positions and calculating drop velocities must be able to distinguish the trajectories of many drops whose images are in the same video frame. We have been developing programs to attain these goals and with a faster computer and video digitization card, it is straightforward to make this improvement.

Another required improvement is to generate drops at a much greater rate. For the next phase of the experiment we have already created a prototype system wherein we are capable of producing a two-dimensional array of drops while

pulsing the dropper at 100–150 Hz. The size of the drops produced is about 7–9 μm. We can control the size of the drops and the rate at which we can produce them consistently.

In the previous paper [8], we discussed the value of levitating a drop after charge measurement if it is a fractional charge candidate. Then the charge can be measured again. This was to be accomplished in [8] by always producing drops with large charges, 10*e* to 20*e*. However, in this experiment, we have found that we get the best precision and more consistent overall operation if the drops have zero or close to zero charge. Therefore, we are developing a method for putting a large charge on a drop after its initial charge has been measured and the drop is considered a fractional candidate. This will be described in another paper.

ACKNOWLEDGMENTS

We want to express our gratitude to Gary Niemi, who worked on the experiment in the difficult early days when we were still using water drops. We also greatly appreciate his setting up of the computer system and the initial programs. We thank Gerard Putallez, Robert Leonard, Ronald Baggs, and Thomas Nakashima for their help in the design and construction of the experiment. We thank the Director of the Research Division of SLAC, David Leith, and the Director of SLAC, Burton Richter, for their support of this speculative experiment. This work was supported by the Department of Energy, Contracts Nos. DE-AC03-76SF00515 and W-7405-ENG-36, Department of Physics, University of California, Irvine.

APPENDIX A: CONTRIBUTION TO THE ERROR IN CHARGE MEASUREMENT FROM BROWNIAN MOTION

The thermal velocity of the drop leads to a random walk with the thermal velocity and a step size that is roughly the stopping distance due to viscous drag. For times Δt much longer than the stopping time, the variation in position is given by [22,23]

$$\Delta z^2 = \frac{2kT}{6\pi\eta r}\,\Delta t.$$

Thus a velocity measurement, given by two position measurements Δt apart, has an uncertainty due to Brownian motion of

$$\Delta v = \sqrt{\frac{kT}{3\pi\eta r\Delta t}} = 8.1\times 10^{-3} \quad \text{mm/s}.$$

This uncertainty in velocity arising from Brownian motion propagates as an uncertainty in the charge calculations according to the equation

$$\sigma_q = \sigma_v c_1 \left\{ (c_2 v_{E_{\text{down}}} + c_3 v_{E_{\text{up}}}) \left(2 + (c_2 - c_3) \times \left[\frac{v_{E_{\text{down}}} - v_{E_{\text{up}}}}{c_2 v_{E_{\text{down}}} + c_3 v_{E_{\text{up}}}} \right] + (c_2^2 + c_3^2) \times \left[\frac{v_{E_{\text{down}}} - v_{E_{\text{up}}}}{2(c_2 v_{E_{\text{down}}} + c_3 v_{E_{\text{up}}})} \right]^2 \right) \right\}^{1/2}, \tag{A1}$$

where we have defined $c_1 = (9\pi d/e)[1/(V_{\text{down}} + V_{\text{up}})]F(T,P)$, $c_2 = V_{\text{up}}/(V_{\text{up}} + V_{\text{down}})$, and $C_3 = V_{\text{down}}/(V_{\text{up}} + V_{\text{down}})$ for convenience and clarity. Since $V_{\text{up}} = V_{\text{down}}$, our equation for the error in charge becomes, upon neglecting the much smaller quadratic term,

$$\sigma_q = \sigma_v c_1 \sqrt{2 v_g}. \tag{A2}$$

Because not all the charge measurements are independent, it was necessary to estimate the error arising from related charge measurements. The first charge measurement is obtained from two independent measurements of velocity v_a and v_b. The second measurement is taken from v_b and v_c and so on with the third and fourth charge measurements. We can calculate an average charge using

$$Q_{\text{ave}} = \tfrac{1}{4}[Q(v_a, v_b) + Q(v_c, v_b) + Q(v_c, v_d) + Q(v_e, v_d)].$$

We assume that each measurement of the velocities has the same error δ. This yields

$$\Delta Q_{\text{ave}} = \delta \sqrt{\left(\frac{\partial Q_{\text{ave}}}{\partial v_a}\right)^2 + \left(\frac{\partial Q_{\text{ave}}}{\partial v_b}\right)^2 + \left(\frac{\partial Q_{\text{ave}}}{\partial v_c}\right)^2 + \left(\frac{\partial Q_{\text{ave}}}{\partial v_d}\right)^2 + \left(\frac{\partial Q_{\text{ave}}}{\partial v_e}\right)^2}. \tag{A3}$$

The partial derivatives can be expressed in terms of those of Q and we find

$$\frac{\partial Q_{\text{ave}}}{\partial v_a} = \frac{1}{4}\left(\frac{\partial Q(v_a, v_b)}{\partial v_a}\right), \quad \frac{\partial Q_{\text{ave}}}{\partial v_b} = \frac{1}{4}\left(\frac{\partial Q(v_a, v_b)}{\partial v_b} + \frac{\partial Q(v_c, v_b)}{\partial v_b}\right),$$

$$\frac{\partial Q_{\rm ave}}{\partial v_c}=\frac{1}{4}\left(\frac{\partial Q(v_c,v_b)}{\partial v_c}+\frac{\partial Q(v_c,v_d)}{\partial v_c}\right),\quad \frac{\partial Q_{\rm ave}}{\partial v_d}=\frac{1}{4}\left(\frac{\partial Q(v_c,v_d)}{\partial v_d}+\frac{\partial Q(v_e,v_d)}{\partial v_d}\right),$$

$$\frac{\partial Q_{\rm ave}}{\partial v_e}=\frac{1}{4}\left(\frac{\partial Q(v_e,v_d)}{\partial v_e}\right).$$

If we make the additional simplifying assumption that the variations in the velocity measurements are sufficiently small (independent of electric field direction), we can evaluate the derivatives at the average values. We obtain

$$\Delta Q_{\rm ave}=\frac{\delta}{4}\sqrt{(\partial_{v_a}Q)^2+4(\partial_{v_b}Q)^2+4(\partial_{v_c}Q)^2+4(\partial_{v_d}Q)^2+(\partial_{v_e}Q)^2}. \tag{A4}$$

We note at this point that $v_a\approx v_c\approx v_e=v_{E_{\rm down}}$ and $v_b\approx v_d=v_{E_{\rm up}}$. Therefore, substituting $v_{E_{\rm down}}$ and $v_{E_{\rm up}}$ for v_a, v_b, v_c, v_d, and v_e where appropriate, Eq. (A4) becomes

$$\begin{aligned}\Delta Q_{\rm ave}&=\frac{\delta}{4}\sqrt{6(\partial_{v_{E_{\rm down}}}Q)^2+8(\partial_{v_{E_{\rm up}}}Q)^2}\\&=\frac{\delta}{4}\sqrt{7((\partial_{v_{E_{\rm down}}}Q)^2+(\partial_{v_{E_{\rm up}}}Q)^2)\left[1-\frac{(\partial_{v_{E_{\rm down}}}Q)^2-(\partial_{v_{E_{\rm up}}}Q)^2}{7[(\partial_{v_{E_{\rm down}}}Q)^2+(\partial_{v_{E_{\rm up}}}Q)^2]}\right]}.\end{aligned} \tag{A5}$$

We assert, however, that the second term in the radicand is negligible since $(\partial_{v_{E_{\rm down}}}Q)^2-(\partial_{v_{E_{\rm up}}}Q)^2\ll(\partial_{v_{E_{\rm down}}}Q)^2+(\partial_{v_{E_{\rm up}}}Q)^2$. This is due to the fact that $(\partial_{v_{E_{\rm down}}}Q)^2\propto v_{E_{\rm down}}$, $(\partial_{v_{E_{\rm up}}}Q)^2\propto v_{E_{\rm up}}$ and $v_{E_{\rm down}}-v_{E_{\rm up}}\ll v_{E_{\rm down}}+v_{E_{\rm up}}$. Equation (A5) then becomes

$$\begin{aligned}\Delta Q_{\rm ave}&=\frac{\delta}{4}\sqrt{7[(\partial_{v_{E_{\rm down}}}Q)^2+(\partial_{v_{E_{\rm up}}}Q)^2]}\\&=\frac{\sqrt{7}\,\delta}{4}\sqrt{(\partial_{v_{E_{\rm down}}}Q)^2+(\partial_{v_{E_{\rm up}}}Q)^2}.\end{aligned} \tag{A6}$$

Similar derivations for the cases where the number of charge measurements is three and five yield factors of $\sqrt{5}/3$ and $\sqrt{9}/5$, respectively. To determine the overall multiplicative factor in our error estimate we add these three factors together in quadrature with their appropriate weights. (Recall that 87.7% of the total number of drops have four charge measurements, 5.9% have three, and 6.4% have five.) The σ_v used in Eq. (A2) has this multiplicative factor taken into account. This gives us an error of 0.021 for a 7.1-μm drop from Brownian motion. Because our errors add in quadrature, Brownian motion accounts for about 70% of our σ_q^2.

APPENDIX B: THE EFFECT OF Q ON CHARGE MEASUREMENT

Using the definitions for c_1, c_2, and c_3 described in the preceding appendix, we note that Eq. (9) can be written as

$$Q=c_1e(v_{E_{\rm down}}-v_{E_{\rm up}})\sqrt{c_2v_{E_{\rm down}}+c_3v_{E_{\rm up}}}. \tag{B1}$$

Solving for the quantity $v_{E_{\rm down}}-v_{E_{\rm up}}$ and substituting this quantity into the error equation, Eq. (A1) becomes

$$\begin{aligned}\sigma_q=\sigma_v c_1\Bigg\{&(c_2v_{E_{\rm down}}+c_3v_{E_{\rm up}})\Bigg(2+(c_2-c_3)\\&\times\left[\frac{Q}{c_1e(c_2v_{E_{\rm down}}+c_3v_{E_{\rm up}})^{3/2}}\right]+(c_2^2+c_3^2)\\&\times\left[\frac{Q}{2c_1e(c_2v_{E_{\rm down}}+c_3v_{E_{\rm up}})^{3/2}}\right]^2\Bigg)\Bigg\}^{1/2}.\end{aligned} \tag{B2}$$

Since $c_2=c_3=\frac{1}{2}$ in this experiment, the above equation can be simplified

$$\sigma_q=\sigma_v c_1\sqrt{v_g\left(2+\left[\frac{Q}{8c_1ev_g^{3/2}}\right]^2\right)} \tag{B3}$$

$$=\sigma_v c_1\sqrt{v_g\left(2+\left[\frac{Q}{30.4e}\right]^2\right)}. \tag{B4}$$

Equation (B4) clearly shows that higher charged drops lead to a greater σ_q.

[1] C. L. Hodges *et al.*, Phys. Rev. Lett. **47**, 1651 (1981).
[2] D. C. Joyce *et al.*, Phys. Rev. Lett. **51**, 731 (1983).
[3] M. A. Lindgren *et al.*, Phys. Rev. Lett. **51**, 1621 (1983).
[4] M. L. Savage *et al.*, Phys. Lett. **167B**, 481 (1986).
[5] R. A. Millikan, Phys. Rev. **32**, 349 (1911).
[6] R. A. Millikan, Philos. Mag. **19**, 209 (1910).
[7] R. A. Millikan, *The Electron* (The University of Chicago Press, Chicago, 1963).
[8] C. D. Hendricks *et al.*, Meas. Sci. Technol. **5**, 337 (1994).
[9] J. Heinzl and C. H. Hertz, *Advances in Electronics and Electron Physics* (Academic, New York, 1985), Vol. 65.
[10] M. Marinelli and G. Morpugo, Phys. Lett. **137B**, 439 (1984).
[11] R. Slansky, T. Goldman, and G. Shaw, Phys. Rev. Lett. **47**, 887 (1981).
[12] G. S. LaRue, J. D. Phillips, and W. M. Fairbank, Phys. Rev. Lett. **46**, 967 (1981).
[13] M. Marinelli and G. Morpurgo, Phys. Rep. **85**, 161 (1982).
[14] D. Liebowitz, M. Binder, and K. O. H. Ziock, Phys. Rev. Lett. **50**, 1640 (1983).
[15] P. F. Smith *et al.*, Phys. Lett. **153B**, 188 (1985).
[16] P. F. Smith, Annu. Rev. Nucl. Part. Sci. **39**, 73 (1989).
[17] R. G. Milner *et al.*, Phys. Rev. Lett. **54**, 1472 (1985).
[18] General Radio Stroboslave Type 1539-A. Quad Tech Inc. Marlboro, MA 01752.
[19] Cohu Model 6310. Cohu Inc. Danville, CA 94526.
[20] N. M. Mar, Ph. D. dissertation, Stanford University, 1996.
[21] *CRC Handbook of Chemistry and Physics*, edited by R. C. Weast, M. J. Astle, and W. H. Beyer (CRC Press, Inc., Boca Raton, FL, 1986).
[22] A. Einstein, in *Investigations on the Theory of the Brownian Movement*, edited by R. Fürth (Dover, New York, 1956).
[23] N. G. van Kampen, *Stochastic Processes in Physics and Chemistry* (North-Holland, Amsterdam, 1981).